

Repeat-Accumulate Signal Codes

Manato Takai, *Student Member, IEEE* and Koji Ishibashi, *Member, IEEE*

Abstract

We propose a new state-constrained signal code, namely *repeat-accumulate signal code* (RASC). The original state-constrained signal code directly encodes modulation signals by signal processing filters, the filter coefficients of which are constrained over the rings of formal power series. Although the performance of signal codes is defined by signal filters, optimum filters were found by brute-force search in terms of symbol error rate (SER) in the literature because the asymptotic behavior with different filters has not been investigated. We introduce Monte Carlo density evolution (MC-DE) to analyze the asymptotic behavior of RASCs. Based on our analysis by MC-DE, the optimum filters can be efficiently found for given parameters of the encoder. Numerical results show the difference between the noise threshold and the Shannon limit is within 0.8 dB. We also introduce a low-complexity decoding algorithm. BCJR algorithm and fast Fourier transform-based belief propagation (FFT-BP) algorithm increase exponentially as the number of output constellations increase. The extended min-sum (EMS) decoder under constraint over the rings is established to overcome this problem. Simulation results show the EMS decoder can reduce the computational complexity to less than 25% of that of BCJR decoder and FFT-BP decoder while the performance loss does not exceed 1 dB.

I. INTRODUCTION

Capacity approaching codes, such as low-density parity check (LDPC) codes and turbo codes, provide significant coding gains [1], [2], [3]. Based on theoretical analysis, the noise thresholds

M. Takai and K. Ishibashi are with Advanced Wireless & Communication Research Center (AWCC), University of Electro-Communications, 1-5-1 Chofugaoka, Chofu-shi, Tokyo 182-8585, Japan e-mail: {manato, koji}@ieee.org

of these codes, which are the maximum decodable noise variances, are close to the Shannon limit. Moreover, simulation results show that these codes exhibit high coding gain over the additive white Gaussian noise (AWGN) channel when binary phase shift keying (BPSK) is used [4], [5]. However, in practice, it is difficult to approach the Shannon capacity because the correlation among unreliable coded bits degrades the decoding performance when high-order modulation is used. Coded modulation is an effective technique for enhancing the coding gain with high-order modulation because this technique enables the Hamming distances of the linear codes and the Euclidean distances of the modulation to be designed in an integrated manner [6], [7]. In order to achieve a high transmission rate, the computational complexity encountered in designing these two distances is impractical because of the enormous number of constellation points involved.

Lattice codes are structured codes for AWGN channels, which have gained a great deal of attention since Urbanke and Rimoldi have proved that lattice codes achieve any rate less than the Shannon capacity with arbitrarily small probability [8]. The advantage of lattice codes is that linear codes over a Hamming space can easily be transformed to Euclidean space by algebraic construction [9]. For instance, Construction A lattices with lattice shaping have been proposed for average power constrained channels [10], [11], [12]. Although the lattices based on Construction A can be decoded by q -ary decoder similar to non-binary codes, q has to be prime so that Construction A is not suitable for typical binary-based communications systems. To overcome this limitation, Construction D has been proposed in [13], which is based on a nested family of binary codes and fits in with the systems. However, the decoder of Construction D consists of not only multiple binary decoders but also corresponding binary encoders, interference cancellers, and modulo operators. This inherent nested architecture obviously leads to the high complexity [14], [15].

Recently, signal codes were proposed as an alternative lattice-coded modulation technique. The entire encoding process consists of simple signal convolution via infinite impulse response (IIR) and/or finite impulse response (FIR) filters. In signal codes, filter coefficients are the most

important parameters for coding gain because the coefficients define Euclidean distances among generated codewords. The authors herein show that the absolute values of filter coefficients must be close to one in order to obtain high coding gain [16]. This implies that the transmission power exponentially increases with codeword length, and shaping techniques such as Tomlinson-Harashima precoding (THP) are necessary to meet average power constraint in practice [17], [18]. Although THP can tailor the transmission power, the number of possible constellation points becomes infinite. This fact results in an exponential decoding complexity, and well-known powerful decoding algorithms such as BCJR algorithm cannot be utilized [19]. Therefore, in [16], a list decoder is used, and the decoding performance is within 2 dB of the Shannon limit, at which the frame error rate (FER) is equal to 10^{-3} . However, list decoding is sub-optimal and is inferior to BCJR algorithm.

Mitran and Ochiai proposed *state-constrained* signal codes called *turbo signal codes* to overcome the explosion of the decoding complexity [20]. In *state-constrained* signal codes, shaping coefficients are chosen over the rings of formal power series. Since rings are closed under addition and multiplication, the output signals are also constrained over the rings, and the possible constellation points become finite. This additional constraint enables the decoder to use the BCJR algorithm, and the resulting performance is within 0.8 dB of the Shannon limit, at which the symbol error rate (SER) is at 10^{-4} . Although the decoding complexity has been relaxed by the rings, turbo signal codes still suffer from a remarkable increase in the number of possible states of filters when higher-order modulation is used as input because the number of states increases exponentially as the order of the modulation increases. This prevents the decoder from using the BCJR algorithm. Moreover, the fundamental code properties of signal codes, such as the noise threshold, have not yet been investigated. Therefore, brute-force search is unavoidable to find the optimum filter coefficients in terms of coding gain [20].

In this paper, in order to address the inherent problems of conventional turbo signal codes, we propose novel state-constrained signal codes, called *repeat-accumulate signal codes* (RASCs).

RASCs are based on repeat-accumulate (RA) codes [21]. The proposed RASCs are composed of a repeater, an interleaver, and a one-tap IIR filter, i.e., an accumulator. Here, the codewords are restricted not only by the rings of formal power series but also by parity check constraints. Although the parity check constraints require density evolution (DE) in order to analyze the noise threshold of the RASCs, regular DE cannot be used because tracking true densities is impractically complex. Hence, we introduce MC-DE [22] for revealing the asymptotic behavior of the RASCs. Thus, the condition for the optimum filter is also studied via MC-DE. Moreover, we introduce a low-complexity decoding algorithm based on the EMS algorithm. The proposed algorithm is modified to decode the codes over the rings of formal power series. The simulation results reveal that the modified EMS can reduce the complexity to a quarter of that of the BCJR algorithm without significant performance loss. In summary, the contributions of the present study are as follows:

- The noise thresholds with several important parameters of RASCs, such as the filter, the parameter of the ring, the column weight, and the input constellation size, are determined via MC-DE. By carefully choosing the parameters, the Shannon capacity is approached to within approximately 0.8 dB.
- A new input constraint is introduced in order to increase the transmission rate. In conventional turbo signal codes, the input signals were constrained by quadrature amplitude modulation (QAM), which is a subset of the rings of formal power series, because providing redundancy in terms of constellation size can be used to improve the error performance [20]. However, our analysis via MC-DE indicates that the noise thresholds when the constellation of the input signals are identical to the ring are slightly better than those when the input signals are constrained by QAM.
- We introduce a modified EMS algorithm for state-constrained signal codes in order to reduce the decoding complexity [23]. The key concept of EMS is to extract only the highly reliable

elements of the message vector in order to reduce the size of the exchanged message vector. As a result, the decoding complexity dramatically decreases because it does not depend on the number of output constellation points but rather on the size of the truncated message vectors. Simulation results show that the performance loss by message truncation does not exceed 1 dB while its computational complexity is less than a quarter of that of the BCJR algorithm or FFT-BP algorithm.

The remainder of this paper is organized as follows. The basics of the signal codes, such as the system model, channel model, and the definition of the rings of formal power series, are explained in Section II. In Section III, we propose the encoding and decoding structure of RASCs. Section IV shows the optimum filters and their noise thresholds as calculated by MC-DE. In Section V, numerical results of RASCs obtained using FFT-BP algorithm and EMS algorithm are presented, and the decoding performances of RASCs and turbo signal codes are compared. Finally, Section VI concludes the paper.

A. Preliminaries

Throughout the paper, expressions of variables are defined as follows; a vector is indicated by boldface with lower case, a matrix is represented by boldface with upper case unless otherwise specified. \mathbb{Z} represents a set of integers, and \mathbb{C} indicates a set of complex numbers. Let $(\cdot)^T$ denote the transpose of a matrix or a vector and $\mathbf{E}[\cdot]$ denote the mean of random variable.

II. BASICS OF SIGNAL CODES

A. Original signal codes

Figure 1 shows a system model of signal codes. Input complex signals $\mathbf{s} = (s_1, s_2, \dots, s_{N_s})^T \in \mathbb{C}^{N_s \times 1}$ are directly encoded by a signal encoder, where N_s is the number of input signals. We assume L^2 -QAM for the input signals, and its constellation is defined as follows:

$$\mathbb{Z}_L[j] = \{v^I + jv^Q : v^I, v^Q \in \{0, 1, \dots, L-1\}\}, \quad (1)$$

where $j = \sqrt{-1}$.

In this paper, Gaussian integer is defined as $\mathbb{Z}[j] = \{a + jb : a, b \in \mathbb{Z}\}$, and thus the input signals are defined as the Gaussian integers modulo L , namely $\mathbb{Z}_L[j] = \{a + jb : a, b \in \mathbb{Z}/L\mathbb{Z}\}$.

The encoder maps input signals to coded signals $\mathbf{x} = (x_1, x_2, \dots, x_{N_c})^T \in \mathbb{C}^{N_c \times 1}$ via a generator matrix $\mathbf{G} \in \mathbb{C}^{N_c \times N_s}$, which has a Toeplitz form as

$$\mathbf{G} = \begin{pmatrix} 1 & 0 & \dots & \dots & 0 & 0 \\ g_1 & 1 & \ddots & \ddots & \vdots & \vdots \\ \vdots & g_1 & \ddots & \ddots & \vdots & \vdots \\ g_p & \vdots & \ddots & \ddots & 1 & \vdots \\ 0 & g_p & \ddots & \ddots & g_p & 1 \\ \vdots & 0 & \ddots & \ddots & \vdots & g_1 \\ \vdots & \vdots & \ddots & \ddots & g_p & \vdots \\ 0 & 0 & \dots & \dots & 0 & g_p \end{pmatrix}, \quad (2)$$

where $1, g_1, g_2, \dots, g_p$ correspond to impulse response coefficients of a FIR filter. Thus the resulting codes are said to be *convolutional lattice codes*. To meet average power constraint, shaping operation should be performed in the encoding process. A shaping vector $\mathbf{b} \in \mathbb{C}^{N_c \times 1}$ restricts the amplitude of encoded signals $x_i, i \in \{1, \dots, N_c\}$ into a desired shaping region. For original signal codes, THP is assumed as the shaping operation. The THP aims to restrict the real and imaginary part of the output constellation into $(-L, L]$. Then the shaping operation is

$$x_t = s_t + \sum_{k=1}^{N_{FF}} g_k (s_{t-k} + b_{t-k}) + b_t \quad (3)$$

where N_F is the number of filter taps, and b_t are chosen as follows:

$$b_t = -2L \left[\frac{1}{2L} \left(s_t + \sum_{k=1}^{N_F} g_k (s_{t-k} + b_{t-k}) \right) \right]. \quad (4)$$

Thus the t th received signal y_t over the AWGN channel can be written by,

$$y_t = x_t + z_t, \quad (5)$$

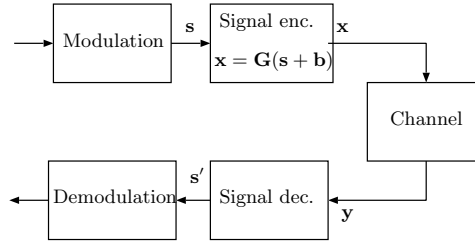


Fig. 1. System model of the signal codes

where z_t is an independent and identically distributed (i.i.d.) circularly-symmetric complex Gaussian random variable with mean zero and variance σ^2 .

B. Turbo signal codes

turbo signal codes introduce the constraint based on the ring of formal power series to control the number of output constellation points. The considered formal power series are given by

$$\mathbb{Z} \left[e^{j \frac{\pi}{2N_{bv}}} \right] = \left\{ \sum_{i=0}^{N_{bv}-1} \left(v_i^I + j v_i^Q \right) e^{j \frac{i\pi}{2N_{bv}}} : v_i^I, v_i^Q \in \mathbb{Z} \right\}, \quad (6)$$

where N_{bv} is an integer indicating the number of possible phase shifts $e^{j \frac{\pi}{2N_{bv}}}$. For shaping operation, the real and imaginary parts of the encoded signal x_i are restricted into $[0, L)$. Moreover, in order to restrict the constellation points to a finite number, the encoded signals are constrained to *the ring of formal power series modulo L* as follows:

$$\begin{aligned} \mathbb{Z}_L \left[e^{j \frac{\pi}{2N_{bv}}} \right] &= \mathbb{Z} \left[e^{j \frac{\pi}{2N_{bv}}} \right] / L \mathbb{Z} \left[e^{j \frac{\pi}{2N_{bv}}} \right] \\ &= \left\{ \sum_{i=0}^{N_{bv}-1} \left(v_i^I + j v_i^Q \right) e^{j \frac{i\pi}{2N_{bv}}} : v_i^I, v_i^Q \in \{0, 1, \dots, L-1\} \right\}. \end{aligned} \quad (7)$$

Then, the t th coded signal of turbo signal codes is given by

$$x_t = \sum_{k=1}^{N_F} f_k u_{t-k} + f_0 \left(s_t + \sum_{k=1}^{N_F} g_k u_{t-k} + b_t \right), \quad (8)$$

$$u_t = s_t + \sum_{k=1}^{N_F} g_k u_{t-k} + b_t \quad (9)$$

where g_k and f_k respectively indicate feedback and feedforward filter coefficients constrained over the ring of formal power series modulo L , and u_{t-k} represents the signal held in the k -th memory of the encoder. All g_k , f_k , and b_t are chosen over $\mathbb{Z}_L \left[e^{j \frac{\pi}{2N_{bv}}} \right]$ so that the encoded signals are constrained over $\mathbb{Z}_L \left[e^{j \frac{\pi}{2N_{bv}}} \right]$ since rings are closed under addition and multiplication. The set of the elements of $\mathbb{Z}_L \left[e^{j \frac{\pi}{2N_{bv}}} \right]$ is defined as $\mathcal{C}(L, N_{bv})$, and the cardinality of $\mathcal{C}(L, N_{bv})$ is obtained by

$$|\mathcal{C}(L, N_{bv})| = L^{2N_{bv}}. \quad (10)$$

The index of feedback filters FB is defined for the short hand notation. From (7), each filter consists of $2N_{bv}$ integer coefficients, v_i^I and v_i^Q for $i = 0, 1, \dots, N_{bv} - 1$. Therefore, if the index of filters is composed of v_i^I and v_i^Q , this index can identify the set of the filter taps. For this reason, the index FB is defined as;

$$\text{FB} = \sum_{j=1}^{N_F} \sum_{i=0}^{N_{bv}-1} \left(v_i^I \times L^{2i+(j-1)*2N_{bv}} + v_i^Q \times L^{2i+1+(j-1)*2N_{bv}} \right). \quad (11)$$

For instance, when the parameters are defined as $L = 2$, $N_{bv} = 2$, $N_F = 1$, and $g_1 = (1+j) + (0+j)e^{j\pi/4}$, the index of the filter can be represented by $\text{FB} = 1 \times 2^0 + 1 \times 2^1 + 0 \times 2^2 + 1 \times 2^3 = 11$.

The index of feedforward filters FF is expressed in the same manner as the FB. Hence,

$$\text{FF} = \sum_{j=0}^{N_F} \sum_{i=0}^{N_{bv}-1} \left(v_i^I \times L^{2i+j*2N_{bv}} + v_i^Q \times L^{2i+1+j*2N_{bv}} \right). \quad (12)$$

III. REPEAT-ACCUMULATE SIGNAL CODES

At least three tap filter coefficients are required to construct turbo signal codes, namely, the tap coefficients of the feedforward filters, f_0 and f_1 , and a tap coefficient of the feedback filter,

g_1 . It is difficult for turbo signal codes to analyze the decoding performance and to design the filter coefficients because the search space of the filter coefficients has a minimum of $L^{6N_{bv}}$ candidates. Therefore, RASCs are proposed in order to reduce the search space to $L^{2N_{bv}}$ because our encoder has only a one tap filter coefficient.

A. Encoding Structure

1) *Encoder*: The encoder of the RASC is shown in Fig. 2. In this paper, non-systematic RASC is assumed so that all information signals are punctured. More specifically, only parity signals are transmitted. The figure shows that the encoder consists of the same components as RA codes. The output signal from the q -times repetition encoder is $\mathbf{c} = (c_1, c_2, \dots, c_{qN_s})^T$, and the output signal from the interleaver is $\mathbf{c}' = (c'_1, c'_2, \dots, c'_{qN_s})^T$, both of which are constrained over the same rings as the input signals \mathbf{s} . For instance, when the input signals are L^2 -QAM, \mathbf{c} and \mathbf{c}' become $(\mathbb{Z}_L[j])^{N_c}$, where $N_c = qN_s$ since non-systematic RASC is assumed. The accumulator of the RASC is slightly different from that of the binary RA because the accumulator consists of a filter and a shaping operation. The t th output signal from the encoder is given by

$$x_t = - (c'_t + g_1 x_{t-1}) + b_t. \quad (13)$$

The resulting codes satisfy the following parity check equation:

$$x_t + c'_t + g_1 x_{t-1} = 0 \pmod{\mathbb{Z}_L \left[e^{j \frac{\pi}{2N_{bv}}} \right]}, \quad (14)$$

where the operation $\pmod{\mathbb{Z}_L \left[e^{j \frac{\pi}{2N_{bv}}} \right]}$ is calculated by a modulo operation for each ring coefficient. Namely, $v_i^I / L\mathbb{Z}$ and $v_i^Q / L\mathbb{Z}$ for $i = 0, 1, \dots, N_{bv} - 1$. The RASC can be decoded by sum-product (SP) algorithm since the parity check matrix can be defined based on (14). On the other hand, conventional turbo signal codes with $L = 2$ and $N_{bv} = 2$ does not meet the parity check equation, so that turbo signal codes cannot be decoded by SP decoder. This proof is presented in details in Appendix A. Note that, to obtain higher coding gain, the following

four parameters must be optimized: the number of repetitions q , the number of phase shifts N_{bv} , the size of input constellation L , and the filter coefficient g_1 .

It is worth noting that, throughout the paper, we assume that the coding rate of RASC is less than half due to non-systematic structure. Although puncturing or combiner can increase the coding rate as similar to binary RA codes, the systematic structure is essential to use these techniques [24].

2) *Transmission Power*: The encoded signals \mathbf{x} are obtained over the ring $\mathbb{Z}_L \left[e^{j \frac{\pi}{2N_{bv}}} \right]$ as described above. This constellation has unnecessarily-high transmission power since the center of this constellation is not at the origin of the complex plane. Therefore, in order to minimize the averaged transmission power, the constellation of the ring is shifted to be centered at the origin. Then, the set of shifted ring is defined as $\tilde{C}(L, N_{bv}) \in \mathbb{C}$. Figure 3 illustrates several signal constellations of $\tilde{C}(L, N_{bv})$. The resulting transmission power of the shifted ring $\tilde{C}(L, N_{bv})$ is given by [20]:

$$E \left[|\mathbf{x}|^2 \right] = \frac{N_{bv} (L^2 - 1)}{6}. \quad (15)$$

3) *Constellation of RASC*: As shown in Fig. 3, the number of signal points appears to increase as L or N_{bv} increases. Several points of $C(L, N_{bv})$ are transformed into the same point of $\tilde{C}(L, N_{bv}) \in \mathbb{C}$ when $N_{bv} > 2$ since the calculation rule of the ring of formal power series is different from that of the complex field. In the ring of formal power series, addition of two elements over $\mathbb{Z}_L \left[e^{j \frac{\pi}{2N_{bv}}} \right]$ can be performed if and only if two elements have the common phase shift $e^{j \frac{i\pi}{2N_{bv}}}$ while addition in the complex field can be done even if they have different phase shifts. For instance, when $L = 2$ and $N_{bv} = 3$, two points $a = (0+j) + (0+0j)e^{j\pi/6} + (0+j0)e^{j2\pi/6}$ and $b = (0+j) + (1+0j)e^{j\pi/6} + (0+j)e^{j2\pi/6}$ cannot be further simplified and thus become different points in the ring of formal power series $C(L, N_{bv}) \in \mathbb{Z}_L \left[e^{j 2N_{bv}} \right]$. However, these points are same when $\tilde{C}(L, N_{bv}) \in \mathbb{C}$, namely $a = b = (0+j)$. Therefore, in Fig. 3-(b) and Fig. 3-(c), the number of constellation points is less than $L^{2N_{bv}}$.

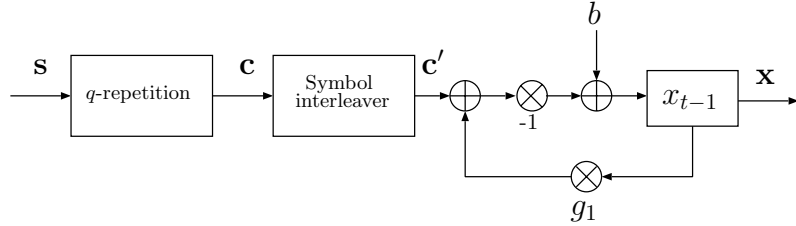
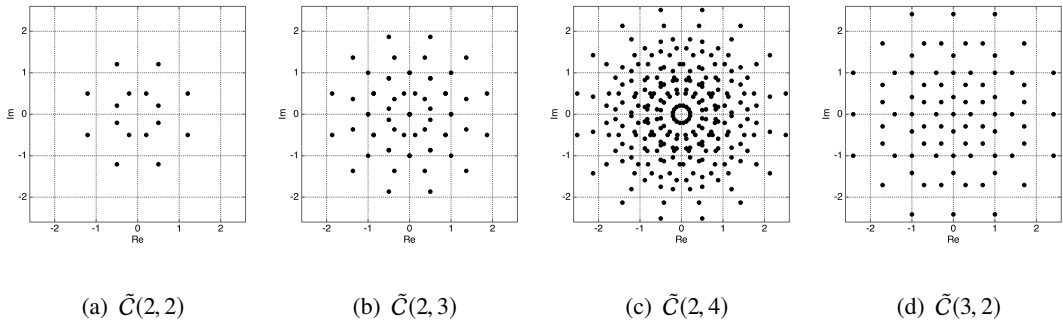


Fig. 2. Encoder of the non-systematic RASC

Fig. 3. Examples of all possible constellation points at the output of the RASC encoder with $\tilde{C}(L, N_{bv})$.

The decoding performance of RASC depends on the filter g_1 because the filter generates different signal constellations as shown in Fig. 4. These figures show various constellations with g_1 for $L = 2$ and $N_{bv} = 2$. It appears from Fig. 3-(a) and Fig. 4-(c) that the constellation generated by $FB = 11$ is same as the ring of formal power series with $L = 2$ and $N_{bv} = 2$. However, from Fig. 4-(a), Fig. 4-(b) and Fig. 4-(d), the generated constellations corresponding to $FB = 3$, $FB = 5$ and $FB = 15$ become a subset of Fig. 3-(a). In the case of the constellation that is a subset of the formal power series, several filtered signal points are degenerated into a few points. This implies that these filters lead to catastrophic codes because degenerated signals cannot be correctly recovered from received signals. Therefore, bijective characteristics are a necessary condition when choosing filters.

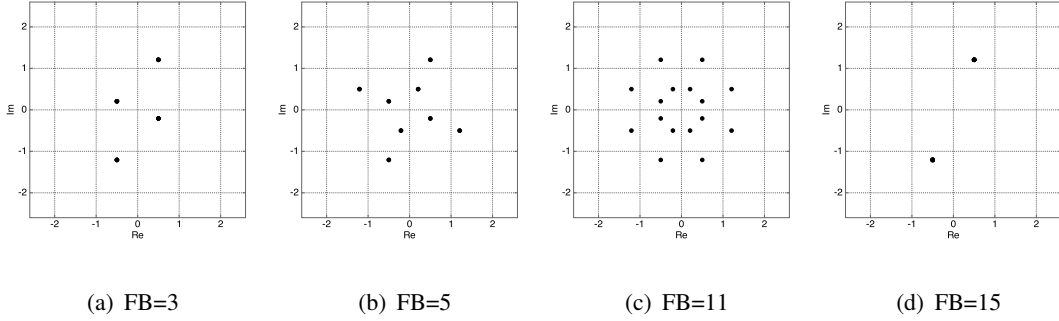


Fig. 4. The filtered signal constellations

of four filters for $\tilde{C}(2, 2)$.

4) *Variable Rate with Variable Input Constraint*: In turbo signal codes, the input signals must be restricted to L^2 -QAM in order to obtain the coding gain. The error correcting capability of turbo signal codes depends on its component codes. When a set of input signals is identical to $\mathbb{Z}_L[e^{j\pi/2N_{bv}}]$, each component code cannot provide any coding gain even if the number of filter taps is infinite as declared in [20]. On the other hand, RASC is based on a serial concatenation of a repetition code and a recursive code so that the coding gain can be obtained even if a set of input signals is identical to $\mathbb{Z}_L[e^{j\pi/2N_{bv}}]$ since the redundancy is introduced by the repetition code. From the definition, $\mathbb{Z}_L[j]$ is a subset of $\mathbb{Z}_L[e^{j\pi/2N_{bv}}]$ as the encoded signals of turbo signal codes. Hence, the input must be restricted to L^2 -QAM namely, $\mathbb{Z}_L[j]$.

The transmission rate of turbo signal codes is defined by the information rate of input L^2 -QAM, namely $\log_2 L^2$ bits per channel use (bpcu). Although L must be increased to achieve a higher rate for turbo signal codes, large L causes high decoding complexity because the number of states is given by $L^{2N_{bv}}$. On the other hand, especially when the input signals are chosen over $\mathbb{Z}_L[e^{j\pi/4}]$, our proposed RASC achieves even higher transmission rate than turbo signal codes for the same L since the cardinality of $\tilde{C}(L, N_{bv})$ is identical to that of $C(L, N_{bv})$ if and only if

$N_{bv} = 2$. Hence, the transmission rate of the non-systematic RASC is given by

$$R_c = \begin{cases} \frac{\log_2 L^2}{q} & \text{if } s \in (\mathbb{Z}_L[j])^{N_s} \\ \frac{\log_2 L^4}{q} & \text{if } s \in \left(\mathbb{Z}_L[e^{j\pi/4}]\right)^{N_s}. \end{cases} \quad (16)$$

B. Decoding Structure

In this subsection, two decoding algorithms, namely FFT-BP algorithm and EMS algorithm, are introduced for the RASC. These algorithms were originally proposed for the purpose of decoding non-binary LDPC defined over a Galois field with low computational complexity. In this paper, we modify these decoding algorithms for RASC defined over $\mathbb{Z}_L[e^{j\pi/2N_{bv}}]$.

1) *FFT-BP Algorithm*: The decoding complexity of the BCJR algorithm for the state-constrained signal codes is $O(L^{4N_{bv}})$, because the number of states in the trellis diagram is given by $L^{2N_{bv}}$. Therefore, a low-complexity decoding algorithm is required especially for large L and N_{bv} , and FFT-BP algorithm is introduced here for the RASC. The complexity of this algorithm is reduced by $O(L^{2N_{bv}} \log_2 L^{2N_{bv}})$.

The exchanged message is defined as a vector of log-likelihood ratios (LLRs), the length of which is $L^{2N_{bv}}$, similar to non-binary LDPC codes. At first, notations to describe FFT-BP algorithm is summarized here.

Notations: In an $m \times n$ parity matrix $\mathbf{H}_{m \times n}$, a set of non-zero elements of the row index at n and a set of non-zero elements of the column index at m are defined as $\mathcal{M}(n) := \{n \mid H_{mn} \neq 0\}$, and $\mathcal{N}(m) := \{m \mid H_{mn} \neq 0\}$, respectively. ℓ represents the number of decoding iteration.

For ease of explanation, the proposed decoding algorithm is explained using a 6×9 small parity check matrix $\mathbf{H}_{6 \times 9}$ in (17). Also, its corresponding bipartite graph is illustrated in Fig. 5. In this figure, the white circles at the top of graph represent variable nodes of information signal, The white square boxes in the middle represent check nodes, and the black circles at the bottom represent the variable nodes of parity signals.

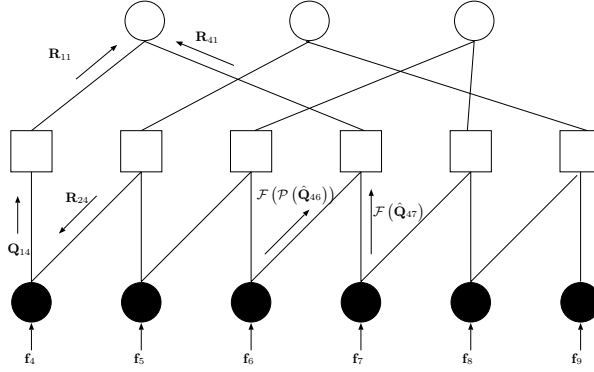


Fig. 5. The bipartite graph of $H_{6 \times 9}$ in (17)

$$H_{6 \times 9} = \begin{bmatrix} 1 & 0 & 0 & 1 & 0 & 0 & 0 & 0 & 0 \\ 0 & 1 & 0 & g_1 & 1 & 0 & 0 & 0 & 0 \\ 0 & 0 & 1 & 0 & g_1 & 1 & 0 & 0 & 0 \\ 1 & 0 & 0 & 0 & 0 & g_1 & 1 & 0 & 0 \\ 0 & 0 & 1 & 0 & 0 & 0 & g_1 & 1 & 0 \\ 0 & 1 & 0 & 0 & 0 & 0 & 0 & g_1 & 1 \end{bmatrix} \quad (17)$$

Message vectors of variable node and check node at H_{mn} are denoted by Q_{mn}^ℓ and R_{mn}^ℓ , respectively. Channel LLR vector is also denoted by f_n . As an example, the message vector of the variable node Q_{mn}^ℓ is given by

$$Q_{mn}^\ell = \left[Q_{mn,a_0}^\ell, \dots, Q_{mn,a_{L^{2N_{bv}-1}}}^\ell \right]^T, \quad (18)$$

where

$$Q_{mn,a_i}^\ell = \log \frac{\Pr(X = a_i)}{\Pr(X = a_0)}, \quad (19)$$

$P(X = a_i)$ is the probability that the random variable X takes on the value $a_i \in \mathbb{Z}_L[e^{j\frac{\pi}{2N_{bv}}}]$ for $i \in \{0, 1, \dots, L^{2N_{bv}} - 1\}$. Also, $Q_{mn,a_0}^\ell = 0$ and $Q_{mn,a_i}^\ell \in \mathbb{R}$. Similarly, R_{mn}^ℓ and f_n are expressed

in the same manner. The four steps of FFT-BP algorithm are described below.

Initialization: As initialization, all elements of Q_{mn}^0 and R_{mn}^0 , and f_n are given by,

$$f_{n,a_i} = \log \frac{P(y_n|X = a_i)}{P(y_n|X = a_0)}, \quad (20)$$

$$Q_{mn,a_i}^0 = 0, \quad (21)$$

$$R_{mn,a_i}^0 = 0, \quad (22)$$

where $P(y_n|X = a_i) = (1/\sqrt{2\pi\sigma^2}) \exp((y_n - a_i)^2/2\sigma^2)$. Note that $f_{n,a_i} = 0, \forall i$ for $n \leq N_s$ in this paper since non-systematic RASC is considered. Thus, as shown in Fig.5, every variable nodes of information signals do not have channel LLRs.

Variable Node Updates: the elements of variable node messages Q_{mn,a_i}^ℓ are updated via following rule:

$$\begin{aligned} Q_{mn,a_i}^\ell &= f_{n,a_i} + \sum_{j \in \mathcal{M} \setminus m} R_{jn,a_i}^{\ell-1} - \alpha_{mn}, \\ \alpha_{mn} &= \max_{a_i} Q_{mn,a_i}^\ell, \end{aligned} \quad (23)$$

where α_{mn} is a term for normalization which achieves numerical stability during iteration. In non-systematic RASC, the variable nodes at $n \leq N_s$ are to be hidden nodes since information signals are not transmitted. If the signals of a hidden node are chosen over $s_i \in \mathbb{Z}_L[j]$, the message is updated as

$$Q_{mn,a_i}^\ell = \begin{cases} f_n + \sum_{j \in \mathcal{M} \setminus m} R_{jn,a_i}^{\ell-1} - \alpha_{mn} & a_i \in \mathbb{Z}_L[j] \\ -\infty & \text{otherwise.} \end{cases} \quad (24)$$

This procedure enables the decoder to ignore impossible candidates since input signals are defined over $\mathbb{Z}_L[j]$. The main difference of modified FFT-BP algorithm from conventional one for non-binary LDPC codes is (24) since the number of input signal constellation can be less than that of output signal constellation. If the input constellation is defined as $\mathbb{Z}_L \left[e^{j \frac{\pi}{2N_{bv}}} \right]$, RASC can be decoded by the same FFT-BP algorithm for non-binary LDPC over $\text{GF}(L^{2N_{bv}})$.

Check Node Updates: the update for both hidden and observation nodes is given by

$$\mathbf{R}_{mn}^\ell = \mathcal{P}^{-1} \left(\mathcal{F}^{-1} \left(\sum_{j \in \mathcal{N} \setminus n} \mathcal{F} \left(\mathcal{P} \left(\mathbf{Q}_{mj}^{\ell-1} \right) \right) \right) \right), \quad (25)$$

where \mathcal{P} indicates permutation function which depends on the filter, \mathcal{F} represents multidimensional FFT function, and, \mathcal{P}^{-1} and \mathcal{F}^{-1} are inverse functions corresponding to \mathcal{P} and \mathcal{F} , respectively. When $L = 2$, \mathcal{F} can be computed by Walsh-Hadamard transform as same as the decoding of non-binary LDPC codes [23]. In addition, as described in [25], there exists Fourier transform if the code are constrained over Abelian groups. Therefore, if L is equal to a power of two, RASC can be decoded via FFT-BP algorithm since the codewords are constrained by the rings of formal power series, which also satisfy the property of commutative additive groups. Note that, in log-domain FFT-BP algorithm, every LLR is splitted into the amplitude and the sign for efficient and stable calculation, but details are omitted here for brevity. For more details, please refer to [26].

Tentative Decision: the information signal at $n = 1, 2, \dots, N_s$, $a \in \mathbb{Z}_L[j]$ is estimated after ℓ_{max} iterations by the following criterion:

$$s'_n = \arg \max_{a_i} f_{n,a_i} + \sum_{j \in \mathcal{M}} R_{jn,a_i}^{\ell_{max}}, \quad (26)$$

In order to elucidate FFT-BP algorithm, update calculations for $\mathbf{H}_{6 \times 9}$ are shown here where the corresponding Tanner graph is depicted in Fig. 5.

The variable node message from the first parity signal (the leftmost black circle) to the first check node (the leftmost white box) is given by,

$$\mathbf{Q}_{14,a_i}^\ell = f_{4,a_i} + R_{24,a_i}^{\ell-1} - \alpha_{41}.$$

Also, the check node message of the first check node (the leftmost white box) to the first information node (the leftmost white circle) is given by,

$$\mathbf{R}_{11}^\ell = \mathbf{Q}_{14}^{\ell-1}. \quad (27)$$

Similar to (27), the check node message of the fourth check node (the fourth white box from the left) can be written by,

$$\mathbf{R}_{41}^{\ell} = \mathcal{F}^{-1} \left(\mathcal{F} \left(\mathbf{Q}_{47}^{\ell-1} \right) + \mathcal{F} \left(\mathcal{P} \left(\mathbf{Q}_{46}^{\ell-1} \right) \right) \right), \quad (28)$$

At the end, The tentative decision of the first information signal (the leftmost white circle) can be computed by,

$$s'_1 = \arg \max_{a_i} R_{11,a_i}^{\ell_{max}} + R_{41,a_i}^{\ell_{max}}. \quad (29)$$

The other information signals can be also recovered in the same manner.

2) *Modified EMS Algorithm*: The FFT-BP algorithm can reduce the decoding complexity to $O(L^{2N_{bv}} \log_2 L^{2N_{bv}})$ if and only if the number of output constellation points is a power of two. However, the decoding complexity increases exponentially by L and N_{bv} . The modified EMS algorithm based on [27] is introduced herein in order to alleviate this complexity issue. The decoding complexities of both the variable node and check node updates can be reduced by each elementary step described below.

Message Truncation:

First, we truncate the message vector for the largest N_m LLRs, denoted by $Q_{mn}[k]$ and $R_{mn}[k]$, $k = 0, 1, \dots, N_m - 1$. The values in these message vectors are sorted in decreasing order. Thus, $Q_{mn}[0] \geq Q_{mn}[1] \geq \dots \geq Q_{mn}[N_m - 1]$ must be satisfied, and also $R_{mn}[k]$ must satisfy the same manner. The corresponding symbol for each $Q_{mn}[k]$ and $R_{mn}[k]$ has to be stored with the message vector. Every step of modified EMS decoder chooses the N_m largest messages, and the decoder has to store the correspondences between symbols and stored messages otherwise the decoder cannot retrieve the original information with partial messages. More specifically, the decoder cannot know which signal corresponds to each $Q_{mn}[k]$ and $R_{mn}[k]$, so that $\beta_{Q_{mn}[k]}$ and $\beta_{R_{mn}[k]}$ hold such information. For example, $\beta_{Q_{mn}[k]} \in \tilde{C}(L, N_{bv})$ stores the symbol corresponding to the message $Q_{mn}[k]$.

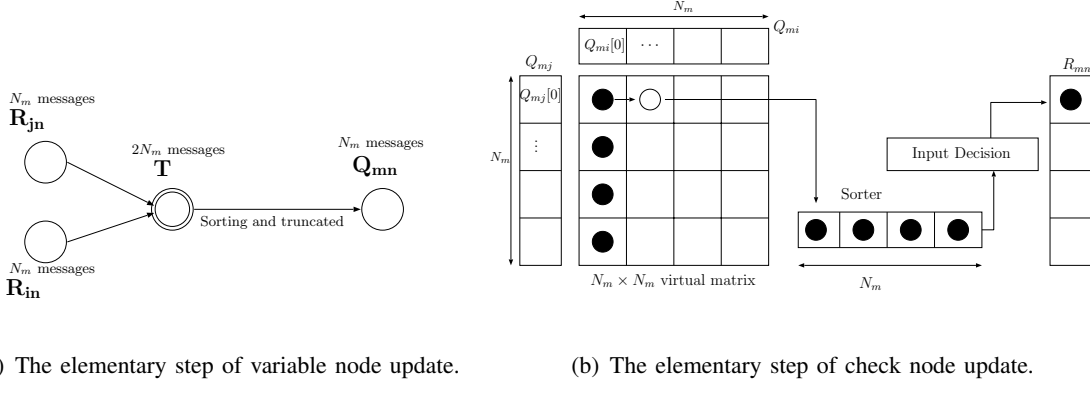


Fig. 6. The elementary steps of variable node and check node updates in the modified EMS algorithm

The decoding complexity can be significantly reduced when $N_m \ll L^{2N_{bv}}$ because only the truncated messages are exchanged.

Elementary Step of Variable Node Update:

A computation of variable node in modified EMS is described. We now assume $q = 2$ for brevity. For $q > 3$, the output of this elementary step is held as an intermediate message, and the step is processed recursively. The variable node updates are illustrated in Fig.6-(a). The decoder firstly computes $2N_m$ message candidates from two sorted message vectors $\mathbf{R}_{m'n}$ and $\mathbf{R}_{m''n}$. These $2N_m$ candidates are temporary stored in a $2N_m$ length message vector \mathbf{T} . The message vector \mathbf{T} is sorted to find N_m reliable messages, and then the k th element of the sorted \mathbf{T} , $\mathbf{T}[k]$ ($k = 0, 1, \dots, N_m - 1$), is moved into the outcoming message $Q_{mn}[k]$. This procedure is denoted as follows;

$$T[k] = R_{m'n}^{\ell-1}[k] + Y_{m''n} \quad (30)$$

$$T[k + N_m] = \gamma_{R_{m'n}} + R_{m''n}^{\ell}[k], \quad (31)$$

where $k = 0, 1, \dots, N_m - 1$. Also, $Y_{m''n}$ is given by

$$Y_{m''n} = \begin{cases} R_{m''n}[l] & \text{if } \beta_{R_{m''n}[l]} = \beta_{R_{m'n}[k]} \\ \gamma_{R_{m''n}} & \text{if } \beta_{R_{m''n}[l]} \neq \beta_{R_{m'n}[k]}, \forall l, k, \end{cases} \quad (32)$$

where $\gamma_{R_{m''n}}$ is a scalar value that compensates for truncated $L^{2N_{bv}} - N_m$ LLRs and is given by

$$\gamma_{R_{m''n}} = R_{m''n}[N_m] - \log(L^{2N_m} - N_m) - \eta, \quad (33)$$

where η is an offset value optimized by density evolution [27]. The variable node message $Q_{mn}[k]$ consists of N_m LLRs from T . If the input signals is defined as $s_i \in \mathbb{Z}_l[j]$, then the hidden node messages are updated by

$$Q_{mn}[k] = \begin{cases} T[l] & \text{if } \beta_{T[l]} \in \mathbb{Z}_L[j] \\ \gamma'_T & \text{if } \beta_{\mathbb{Z}_L[j]} \neq \beta_{T[l]}, \forall l \\ -\infty & \text{otherwise,} \end{cases} \quad (34)$$

where $\beta_{\mathbb{Z}_L[j]} = \{a_0, \dots, a_{L^2}\}$ represents all possible symbols defined over $\mathbb{Z}_L[j]$, and γ'_T is given by

$$\gamma'_T = T[l_z] - \log(L^{2N_m} - l_z) - \eta, \quad (35)$$

where l_z represents the largest index of LLR corresponding symbol is $\beta_{T[l_z]} \in \mathbb{Z}[j]$. This algorithm is slightly different from the original EMS algorithm for non-binary LDPC codes since the decoder has *a priori* knowledge of input signals which are constrained over $\mathbb{Z}_L[j]$. Therefore, the decoder replaces the LLR with negative infinity when the corresponding input signal is not in $\mathbb{Z}_L[j]$. Also, the decoder replaces the LLR with a constant value γ'_T when the corresponding symbol is not in $\beta_{T[l]}$ for $\forall l$. When the input signals are constrained over the rings of formal power series modulo L , then the decoder naively updates the variable messages via (31).

Elementary Step of Check Node Update:

Similar to the variable node update, the output of this elementary step is stored as an intermediate message and recursively updates when the row degree is greater than three. For simplify,

we assume that the row degree is two without loss of generality. Let $R_{mn}[k]$ be the outgoing message. $Q_{mn'}[k']$ and $Q_{mn''}[k'']$ are incoming messages to evaluate $R_{mn}[k]$. In the check node updates, the decoder computes the outgoing message vector from a set $\mathcal{S}(\beta_{R_{mn}[k]})$ defined as the all possible signal combinations which satisfy the parity equation $\beta_{Q_{mn'}[k']} + \beta_{Q_{mn''}[k'']} + \beta_{R_{mn}[k]} = 0 \pmod{\mathbb{Z}_L[e^{j\frac{\pi}{2N_{bv}}}]}$ as follows;

$$R_{mn}[k] = \max_{\mathcal{S}(\beta_{R_{mn}[k]})} (Q_{mn'}[k'] + Q_{mn''}[k'']), \quad k, k', k'' \in \{0, 1, \dots, N_m - 1\}$$

If the decoder naively searched the candidates of the set, the computational complexity would be $O(N_m^2)$. Then, to reduce the computational complexity, an $N_m \times N_m$ virtual matrix illustrated in Fig. 6-(b) is introduced. The element of this virtual matrix at (k', k'') can be computed as $Q_{mn'}[k'] + Q_{mn''}[k'']$. The messages exist at the upper left in the virtual matrix are more reliable than the messages exist at the lower right in the virtual matrix because two incoming messages $Q_{mn'}[k']$ and $Q_{mn''}[k'']$ are sorted. Thus, the decoder can compute the outgoing message $R_{mn}[k]$ by finding N_m messages from the upper left in the virtual matrix to the lower right in the virtual matrix. This algorithm is as follows;

- 1) Introduce the values of the first column of the virtual matrix to the sorter.
- 2) Compute the largest value in the sorter.
- 3) Does the symbol associated with the largest output value exist in the output vector?
 - Yes: Remove the largest output value from the sorter.
 - No: Append the largest output value to the last element of the output vector.
- 4) Move to the right neighbor of the largest value in the message matrix to the sorter.

The above check node update does not stop after N_m steps because the number of element of the output vector does not reached N_m due to existing the same symbols at Step 3 within N_m steps. However, $2N_m$ steps are sufficient for a negligible degradation in decoding performance [27].

IV. NOISE THRESHOLD ANALYSIS AND FILTER DESIGN

A. Monte Carlo Density Evolution

Density evolution is a powerful tool for finding the noise threshold, which is an important indicator of code performance characteristics. In binary codes, the mathematical formulation of DE is easily obtained because the belief-propagation (BP) messages are scalars [1], [2]. In the non-binary case, tracking the true BP message distribution is impractically complex because the BP messages are vectors. *Gaussian approximation* (GA) is a feasible way to track the density of BP messages for non-binary LDPC codes because it can reduce the number of parameters to only two, namely the mean and the variance of the density [28]. However, the message distribution of the check node diverges increasingly from the true distribution as the degree of the check node increases. Furthermore, GA can be used if and only if *channel symmetry* and *permutation invariance* can be assumed [29]. Channel symmetry leads to an uncorrelated message distribution, so that the all-zero codeword assumption may be valid. Permutation invariance means eliminating the effect of the weight of the parity matrix, which is obtained by a random weight coefficient. In state-constrained signal codes, the BP messages also consist of multiple LLRs, and the decoding performance depends on the codewords because of the asymmetric property of non-uniform modulation. Therefore, we introduce the technique of adding a random coset vector, as described in [28]. The random-coset vector is added at the end of the encoder. The random-coset elements are randomly chosen and uniformly distributed over $\mathbb{Z}_L [e^{j\pi/2N_{bv}}]$. Thus, the resulting output codeword from the AWGN channel is symmetric. The proof of this symmetric property resulting from the random-coset vector is omitted herein. (Please refer to [28] for the proof.) Although the channel symmetry can be assumed, permutation invariance cannot be assumed because the weight coefficients are defined by the IIR filter coefficient. MC-DE has been introduced as alternative approach for tracking the density with multiple parameters [22], [30], [31]. One advantage of MC-DE is that the estimated noise threshold is more accurate than

the Gaussian approximation method because the analysis is non-parametric [22]. Thanks to the random-coset settings for the RASC, as described above, we can straightforwardly introduce MC-DE to approximate the noise threshold σ_{th} . We now briefly describe the MC-DE algorithm. Four kinds of message pools Q^I , Q^P , R^I , and R^P correspond to variable node messages of information signals, variable node messages of parity signals, check node messages of information signals, and check node messages of parity signals, respectively. Every message pool has N_{sam} messages. Message updates are performed by modified FFT-BP algorithm described in Sec. III-B. When the check node message of parity signal is calculated, the variable node message of information signal and the variable node message of parity signal are uniformly picked up from the message pool Q^I and Q^P , respectively. Then, the updated check node message of parity signal become an input message to calculate the variable node message of parity signal in R^P . The other message updates can be also conducted based on the FFT-BP algorithm with the four message pools.

The parameters we set to calculate the noise threshold of RASC are as follows: the number of the noise threshold calculations, $R_{max} = 10$; the number of message samples, $N_{sam} = 5000$; maximum number of iterations, $\ell_{max} = 100$; decoding error threshold, $P_{th} = 10^{-4}$, which means that decoding could be regarded as successful when all symbols are correctly decoded; and the noise threshold precision value, $\epsilon_{\sigma} = 10^{-5}$, which is used for termination of bisection method. If the interval of searched noise variance is less than ϵ_{σ} , bisection search algorithm is stopped. In the subsequent section, we present the results of the optimum parameters and the corresponding noise threshold.

B. Searching for the Best Filter

As described in the Introduction, an efficient search algorithm for the filter coefficient of state-constrained signal codes has not been reported [20]. As shown in Fig.4, several filters whose property is not bijective generate undecodable codewords. Therefore, the proposed search algorithm computes the noise thresholds for only bijective filters so that the number of candidate

filter is less than $L^{2N_{bv}}$.

In order to clarify the property of relations among filters, the several results that the best four filters with several parameters found by MC-DE are shown in Table I and Table II. Several filters exhibit same or almost same noise thresholds. For instance, in Table I, FB = 28 and FB = 44 have the same noise threshold (0.79 dB). Similarly, FB = 52 and FB = 56 have the same noise threshold (0.80 dB). The same relationships can be found in Table II. These filters are converted by affine transformation with each other, e.g., by rotation by 90 degrees, extension, and reduction. This property can be exploited so as to further reduce the number of candidate filters.

TABLE I

BEST FOUR FILTERS FOR $L = 2, N_{bv} = 3$, AND $q = 2$.

FB	Taps	Threshold [dB]
28	(0,0),(1,1),(1,0)	0.79
44	(0,0),(1,1),(0,1)	0.79
52	(0,0),(1,0),(1,1)	0.80
56	(0,0),(0,1),(1,1)	0.80

TABLE II

BEST FOUR FILTERS FOR $L = 3, N_{bv} = 2$, AND $q = 2$.

FB	Taps	Threshold [dB]
45	(0,0),(2,1)	3.85
63	(0,0),(1,2)	3.85
36	(0,0),(1,1)	3.86
72	(0,0),(2,2)	3.86

C. Noise Thresholds for various N_{bv}

Figure 7 shows the difference between the noise threshold of the RASC and the Shannon limit. In this paper, the Shannon limit is calculated by the channel capacity with Gaussian input distribution. This figure clarifies the impact of N_{bv} on the noise threshold. The indices of the best filters for each N_{bv} are shown in this figure because different values of N_{bv} have different optimum filters. Note that some affine transformed filters have the same noise threshold, as described above. Thus, the filters must be searched for every target N_{bv} . Furthermore, the number of repetitions q must be optimized for each N_{bv} . Based on our results, the optimal value

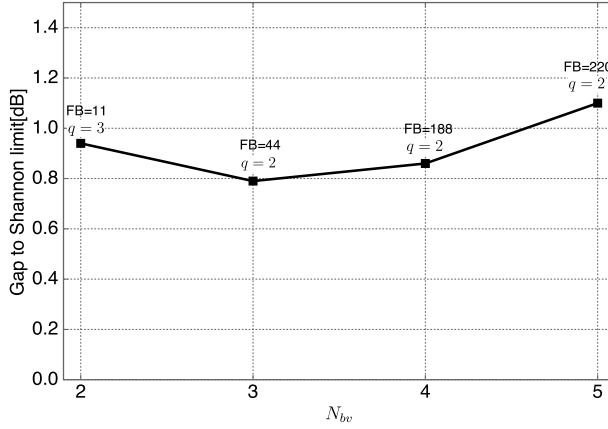


Fig. 7. The noise thresholds of various N_{bv} with $L = 2$.

of q is three for $N_{bv} = 2$, whereas that for $N_{bv} \geq 3$ is two. In non-binary LDPC, the optimum column weight is two for a large alphabet size, e.g., greater than or equal to GF(64) [32].

Unfortunately, the noise threshold does not improve monotonically as N_{bv} increases. We believe that the reason for which is the dense constellation of output signals. As shown in Figs. 3-(a), 3-(b), and 3-(c), the distance between the signal points decreases as N_{bv} increases. Thus, increasing N_{bv} improves coding gain but results in a short Euclidean distance of the constellation.

D. Noise Thresholds for Different Numbers of Repetitions

The effect of the number of repetitions q is shown in Fig. 8. Similar to the previous results, the optimum filter varies depending on q . The difference between the noise threshold of the RASC and the Shannon limit for $N_{bv} = 3$ and FB = 44 is the smallest among all other parameters at $q = 2$ ($= 0.79$ dB). However, for $q \geq 3$, the noise thresholds for $N_{bv} = 3$ are inferior to those for $N_{bv} = 2$. This conclusion can also be found in the literature on non-binary LDPC code, where for a column weight greater than three, the performance of the codes over higher-order fields is

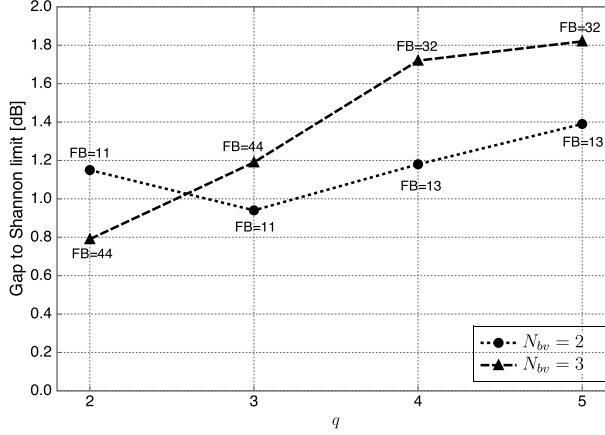


Fig. 8. The noise thresholds of various q for $L = 2$ with $N_{bv} = 2$ and $N_{bv} = 3$.

worse than that of the codes over lower-order fields [32].

E. Noise Thresholds for Different Input Constellation Sizes

The impact of the input constellation size L is shown in Fig. 9. Since the computational complexity required for $L \geq 3$ with $N_{bv} \geq 3$ is enormous, only the case of $N_{bv} = 2$ is illustrated. In this figure, according to the discussion about the optimum q in the previous subsection, $q = 3$ is used for $L = 2$, and $q = 2$ is used for $L = 3, 4$. In contrast to the impact of N_{bv} , the difference between the noise threshold of the RASC and the Shannon capacity decreases as L increases. The reason for this behavior, which differs from that for increasing N_{bv} , is that the distances between the output signals are greater than for fixed L because the signal constellation space is expanded by L . Based on this result, the RASC appears to have the excellent property whereby increasing the transmission rate improves the noise threshold.

F. Noise Threshold for Different Input Constraints

Finally, the effect of the input signal constraint is shown in Fig. 10. In this case, the optimum filters for the same q and N_{bv} differ depending on the constraint. Interestingly, FB = 1, which

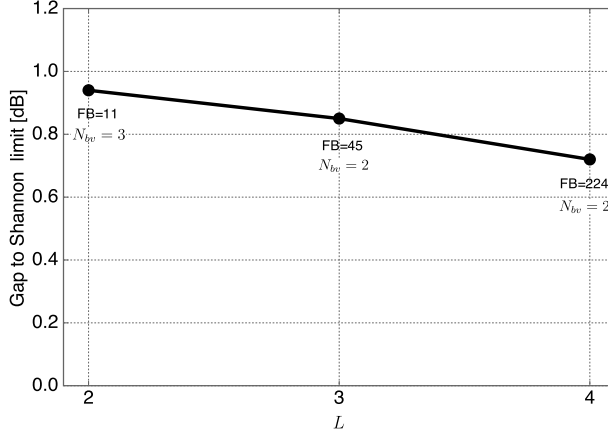


Fig. 9. The noise thresholds for different input constellation sizes L . $q = 3$ is used for $L = 2$, and $q = 2$ is used for $L = 3, 4$.

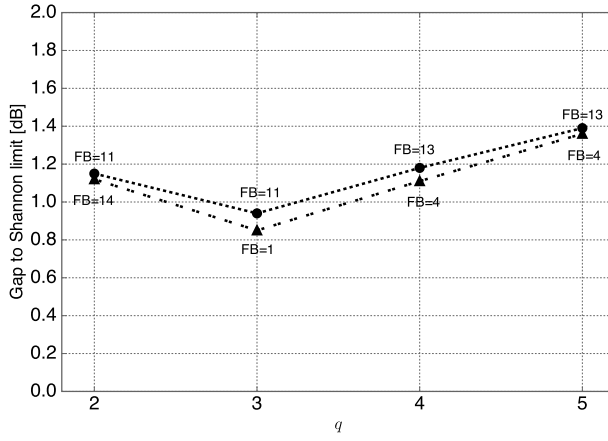


Fig. 10. Noise thresholds for different input constraints for $L = 2$ and $N_{bv} = 2$

is an identity mapping function, is the best filter for $q = 3$ and $L = N_{bv} = 2$. We believe that the reason for this is that when the input signals are chosen over $\mathbb{Z}_L[e^{j\frac{\pi}{2N_{bv}}}]$, the transition of the state due to the summation of signals is chosen over $\mathbb{Z}_L[e^{j\frac{\pi}{2N_{bv}}}]$. Then, the codeword distances increase, even if the signals are mapped into the same mapping space by $FB = 1$.

V. NUMERICAL RESULTS

In this section, the finite length performances of the RASC are shown. We assume that the interleaver of the encoder is a random interleaver, the number of iterations of FFT-BP algorithm is 100, and the filters are chosen as described in the previous section.

A. Performance of the RASC with FFT-BP

Figure 11 shows the SER of finite-codeword-length RASC with FFT-BP decoding. The input signals are 4-QAM ($L = 2$) with length $N_s = 1000$, and the filters are chosen as FB = 11 and FB = 44 for $N_{bv} = 2$ and $N_{bv} = 3$, respectively. As shown in the figure, the relationship between N_{bv} and q is the same as that determined by a previous noise threshold analysis. Namely, for $N_{bv} = 2$, the performance for $q = 3$ is superior to that for $q = 2$ in both the waterfall and error floor regions. In contrast, for $N_{bv} \geq 3$, the noise threshold of $q = 3$ is inferior to that of $q = 2$. Interestingly, the performance for the error floor region depends on the filter but not the number of states. Therefore, the best filter can only be chosen if we find the best noise threshold via MC-DE, because the overall performance is defined by the filter.

Next, we compare the performance of the RASC with that of the turbo signal codes where $N_s = 1000$, $L = 2$, and $N_{bv} = 2$ for both codes. Due to a termination, the transmission rates of the RASC and the turbo signal codes are $R_{RASC} = 2 \times \frac{1000}{2000+1} = 0.9995$ bpcu. and $R_{turbo} = 2 \times \frac{1000}{2000+8} = 0.9960$ bpcu, respectively. For the turbo signal codes, we assume that the indices of the feedback and feedforward filters are FB=11 and FF=81, respectively. This optimum filter setting was reported in [20]. The decoding algorithm is the BCJR algorithm, and the number of iterations is 25. The order of computational complexity per a decoding iteration of BCJR and FFT-BP are $O(L^{4N_{bv}})$ and $O(L^{2N_{bv}} \log_2 L^{2N_{bv}})$, respectively. Thus, for $L = 2$ and $N_{bv} = 2$, the computational cost of BCJR is four times higher than FFT-BP. Therefore, BCJR with 25 iterations and FFT-BP with 100 iterations are the equal setting in terms of the decoding complexity. As shown in Fig. 11, the performance of the RASC with $N_{bv} = 2$ is close to that of turbo signal codes

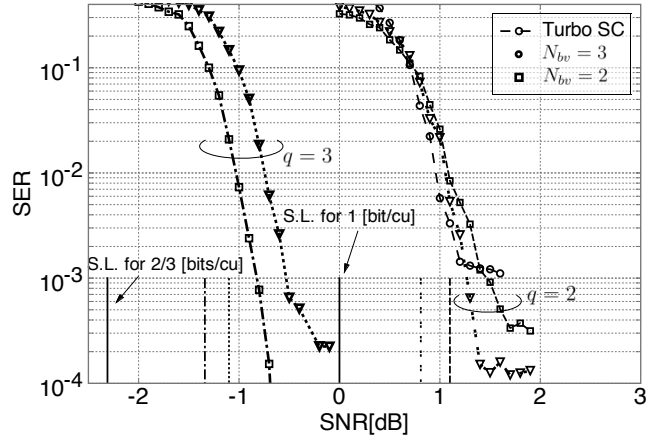


Fig. 11. Performances of the optimized filter for $L = 2$ and $N_{bv} = 2, 3$. The filter index is FB = 11 for $N_{bv} = 2$ and FB = 44 for $N_{bv} = 3$. The solid lines indicate Shannon limits, and the other lines (chain, dot, twin, and dashed) indicate the noise thresholds corresponding to the same kinds of curves of SER.

(within 0.2 dB, which is a negligible performance loss) in the waterfall region. Furthermore, in the error floor region, the error probability of the RASC is approximately 1/3 better than that of the turbo signal codes. These results indicate that the RASC can provide superior performance to turbo signal codes with only a one-tap feedback filter.

We finally mention the performance loss of our designed codes compared with the Shannon limit. The authors in [20] show that the mutual information for the constellations of $\tilde{C}(L, N_{bv})$ can almost achieve the channel capacity with Gaussian input distribution at the transmission rate equal to 1 bpcu [20, Fig. 3]. This implies that the shaping loss of RASC is negligible, and thus the gap between the noise threshold of RASC and the Shannon limit mainly comes from the coding loss.

B. Performance of the RASC with EMS

Figure 12 shows the SER performance for $L = 3$ and $L = 4$ obtained using the proposed modified EMS decoder. We assume that $N_{bv} = 2$, $q = 2$, and $N_s = 1000$. In this figure, the dotted line and the chained line indicate the noise threshold for $L = 3$ and $L = 4$ with the optimized filters. *Full BP* indicates the naive sum-product algorithm whereby all sets of the signals that satisfy the check equation are searched and calculated for the message updates in check nodes so that the decoder does not use FFT-BP algorithm since FFT algorithm over the rings of formal power series modulo L with $L > 2$ cannot be represented by multidimensional FFT form as that with $L = 2$. The number of output constellation points $L^{2N_{bv}}$ for $L = 3$ and $L = 4$ are 81 and 256, respectively. The decoding complexities of BCJR algorithm, FFT-BP algorithm, and EMS algorithm are $O(L^{4N_{bv}})$, $O(L^{2N_{bv}} \log_2 L^{2N_{bv}})$, and $O(N_m \log_2 N_m)$, respectively. Therefore, the decoding complexity of EMS can be reduced if N_m is chosen so as to be much smaller than $L^{2N_{bv}}$. For example, when $N_m = L^{2N_{bv}}/2$, the decoding complexity of EMS becomes a quarter of that of the BCJR algorithm, and when $N_m = L^{2N_{bv}}/4$, the decoding complexity of the EMS becomes one-sixteenth that of the BCJR algorithm and a quarter of that of FFT-BP algorithm. Therefore, in this section, $N_m = 40$ and $N_m = 20$ are set for $L = 3$ and, $N_m = 128$ and $N_m = 64$ are set for $L = 4$. Figure 12 indicates that the performance loss is about 0.5 dB when $N_m = L^{2N_{bv}}/2$ and is about 1.0 dB when $N_m = L^{2N_{bv}}/4$. Furthermore, our algorithm does not degrade the error floor performance because the curves with the EMS decoder decrease until reaching the error floor of full BP. As a result, the EMS decoder can dramatically reduce the decoding complexity without significant performance loss.

VI. CONCLUSION

In this paper, we proposed a new state-constrained signal code based on RA codes. The proposed code has several advantages, including a simpler encoder and decoder, as compared to turbo signal codes, with approximately the same performance in the waterfall region and

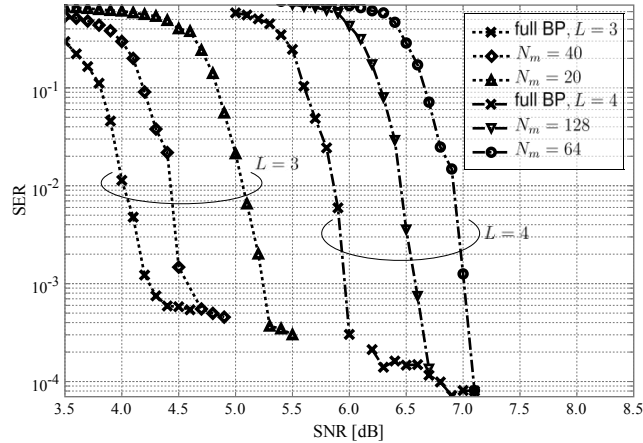


Fig. 12. Performance with the EMS decoder for different values of L and N_m . For all curves, $N_{bv}=2$. The filter index is FB = 45 for $L = 3$ and FB = 224 for $L = 4$. $\eta = \{-3.0, -3.5, -4.7, -5.5\}$ for $N_m = \{20, 40, 64, 128\}$, respectively. The solid lines indicate Shannon limits for each L . The dotted line and the chained line indicate the noise threshold for $L = 3$ and $L = 4$, respectively.

a slightly better performance in the error floor region. Furthermore, we have found a design criterion of the filter coefficient via MC-DE. We summarize the properties of the noise threshold in terms of the following three parameters:

- 1) The parameter of the ring of formal power series N_{bv} can make improve the noise threshold, but an excessive value of N_{bv} leads to a noise threshold degradation.
- 2) An optimum repetition number q exists for a given N_{bv} . In particular, for a large number of states, $L^{2N_{bv}} \geq 64$, $q = 2$ is optimum in terms of the noise threshold.
- 3) The number of states L can improve both the transmission rate and the noise threshold.

Simulation results have shown that the optimum filters for given values of N_{bv} , q , and L perform well in the waterfall and error floor regions with short codeword lengths. Overall performance optimization for the regular RASC can be performed by MC-DE. Furthermore, we proposed a

modified EMS decoder. Simulation results indicate that the performance loss due to the modified EMS decoder is less than 1 dB as compared to the performance of the full BP decoder, while the decoding complexity is reduced to less than 25% of that of BCJR algorithm and FFT-BP algorithm. Finally, the proposed code can be easily generalized to irregular codes and other turbo-like codes, such as accumulate-repeat-accumulate codes and braided convolutional codes, to more closely approach the Shannon limit.

APPENDIX A
NECESSARY CONDITION TO SATISFY THE PARITY CHECK EQUATION
IN TURBO SIGNAL CODES

For simplify, the encoder that has two feedforward filters and one feedback filter is considered as follows:

$$x_t = f_1 u_{t-1} + f_0 (s_t + g_1 u_{t-1} + b_t). \quad (36)$$

In this setting, the parity check matrix of (36) is given by

$$\left[\begin{array}{cccccc|cccccc} 1 & 0 & 0 & \cdots & 0 & 0 & 0 & 1 & 0 & 0 & \cdots & 0 & 0 & 0 \\ 1 & 1 & 0 & \ddots & 0 & 0 & 0 & 1 & 1 & 0 & \ddots & 0 & 0 & 0 \\ 0 & 1 & 1 & \ddots & 0 & 0 & 0 & 0 & 1 & 1 & \ddots & 0 & 0 & 0 \\ 0 & 0 & 0 & \ddots & 1 & 1 & 0 & 0 & 0 & 0 & \ddots & 1 & 1 & 0 \\ 0 & 0 & 0 & \ddots & 0 & 1 & 1 & 0 & 0 & 0 & \ddots & 0 & 1 & 1 \end{array} \right], \quad (37)$$

where the left-hand side of this matrix represents information signals, and the right-hand side represents parity signals. From this matrix, the parity check equation at $t = 1$ is given by

$$s_0 + s_1 + x_0 + x_1 = 0 \pmod{\mathbb{Z}_L \left[e^{j\pi/2N_{bv}} \right]}. \quad (38)$$

From (36), the reformulation of (38) is given by

$$(1 + f_0 + f_0 g_1 + f_1) s_0 + (1 + f_0) s_1 = 0 \pmod{\mathbb{Z}_L \left[e^{j\pi/2N_{bv}} \right]}. \quad (39)$$

Therefore, the filters to satisfy above parity check equation must be $f_0 = -1 + j0 \pmod{\mathbb{Z}_L [e^{j\pi/2N_{bv}}]}$ and $f_1 = g_1$.

For $L = 2$, the coded signal at t is given by

$$x_t = f_1 u_{t-1} + (s_t + f_1 u_{t-1} + b_t) = s_t. \quad (40)$$

Therefore, in turbo signal codes, there is no coding gain if the signals are constrained by parity check equation. This is because the filter does not effect to the input signal as shown in (40).

REFERENCES

- [1] T. J. Richardson and R. L. Urbanke, "The Capacity of Low-Density Parity-Check Codes under Message-Passing Decoding," *IEEE Trans. Inf. Theory*, vol. 47, no. 2, pp. 599–618, 2001.
- [2] S.-Y. Chung, G. D. Forney, T. J. Richardson, and R. Urbanke, "On the Design of Low-Density parity-check codes within 0.0045 dB of the Shannon limit," *IEEE Commun. Lett.*, vol. 5, no. 2, pp. 58–60, 2001.
- [3] S. ten Brink, "Convergence Behavior of Iteratively Decoded Parallel Concatenated Codes," *IEEE Trans. Commun.*, vol. 49, no. 10, pp. 1727–1737, 2001.
- [4] T. J. Richardson, M. A. Shokrollahi, and R. L. Urbanke, "Design of Capacity-Approaching Irregular Low-Density Parity-Check Codes," *IEEE Trans. Inf. Theory*, vol. 47, no. 2, pp. 619–637, 2001.
- [5] C. Berrou, A. Glavieux, and P. Thitimajshima, "Near Shannon limit error-correcting coding and decoding: Turbo-codes. 1," in *Proc. of IEEE ICC 1993*, vol. 2, 1993, pp. 1064–1070 vol.2.
- [6] G. Ungerboeck, "Channel coding with multilevel/phase signals," *IEEE Trans. Inf. Theory*, vol. 28, no. 1, pp. 55–67, 1982.
- [7] G. Caire, G. Taricco, and E. Biglieri, "Bit-Interleaved Coded Modulation," *IEEE Trans. Inf. Theory*, vol. 44, no. 3, pp. 927–946, 1998.
- [8] R. Urbanke and B. Rimoldi, "Lattice codes can achieve capacity on the awgn channel," *IEEE Transactions on Information Theory*, vol. 44, no. 1, pp. 273–278, 1998.
- [9] J. H. Conway and N. J. A. Sloane, *Sphere packings, lattices and groups*. Springer Science & Business Media, 2013, vol. 290.
- [10] H. Khodaiemehr, M. R. Sadeghi, and A. Sakzad, "Practical Encoder and Decoder for Power Constrained QC LDPC-Lattice Codes," *IEEE Trans. Commun.*, vol. 65, no. 2, pp. 486–500, 2017.
- [11] N. di Pietro and J. J. Boutros, "Leech Constellations of Construction-A Lattices," *IEEE Trans. Commun.*, vol. 65, no. 11, pp. 4622–4631, 2017.
- [12] M. Qiu, L. Yang, Y. Xie, and J. Yuan, "On the Design of Multi-Dimensional Irregular Repeat-Accumulate Lattice Codes," *IEEE Trans. Commun.*, vol. 66, no. 2, pp. 478–492, 2018.
- [13] E. S. Barnes and N. J. A. Sloane, "New Lattice Packings of Spheres," *Can. J. Math*, vol. 35, no. 1, pp. 117–130, 1983.
- [14] A. Sakzad, M. Sadeghi, and D. Panario, "Turbo lattices: Construction and performance analysis," *CoRR*, vol. abs/1108.1873, 2011. [Online]. Available: <http://arxiv.org/abs/1108.1873>
- [15] M. R. Sadeghi, A. H. Banihashemi, and D. Panario, "Low-density parity-check lattices: Construction and decoding analysis," *IEEE Trans. Inf. Theory*, vol. 52, no. 10, pp. 4481–4495, 2006.
- [16] O. Shalvi, N. Sommer, and M. Feder, "Signal codes: Convolutional lattice codes," *IEEE Trans. Inf. Theory*, vol. 57, no. 8, pp. 5203–5226, Aug 2011.
- [17] M. Tomlinson, "New automatic equaliser employing modulo arithmetic," *Electronics Letters*, vol. 7, no. 5, pp. 138–139, 1971.
- [18] H. Harashima and H. Miyakawa, "Matched-Transmission Technique for Channels With Intersymbol Interference," *IEEE Trans. Commun.*, vol. 20, no. 4, pp. 774–780, 1972.
- [19] F. R. Kschischang, B. J. Frey, and H. A. Loeliger, "Factor Graphs and the Sum-Product Algorithm," *IEEE Trans. Inf. Theory*, vol. 47, no. 2, pp. 498–519, 2001.

- [20] P. Mitran and H. Ochiai, "Parallel concatenated convolutional lattice codes with constrained states," *IEEE Trans. Commun.*, vol. 63, no. 4, pp. 1081–1090, 2015.
- [21] D. Divsalar, D. Jin, and R. McEliece, "Coding theorems for turbo-like codes," in *Allerton Conference*, 1998, pp. 201–210.
- [22] M. Gorgolione, "Analysis and Design of Non-Binary LDPC Codes over Fading Channels," Ph.D. dissertation, Cergy-Pontoise Univ., 2012.
- [23] D. Declercq and M. Fossorier, "Decoding Algorithms for Nonbinary LDPC Codes Over $GF(q)$," *IEEE Trans. Commun.*, vol. 55, no. 4, pp. 633–643, 2007.
- [24] S. Johnson, *Iterative Error Correction: Turbo, Low-Density Parity-Check and Repeat-Accumulate Codes*. Cambridge University Press, 2009.
- [25] A. Goupil, M. Colas, G. Gelle, and D. Declercq, "FFT-Based BP Decoding of General LDPC Codes Over Abelian Groups," *IEEE Trans. Commun.*, vol. 55, no. 4, pp. 644–649, 2007.
- [26] G. J. Byers and F. Takawira, "Fourier Transform Decoding of Non-Binary LDPC Codes," in *Proc. of SATNAC. Spier Wine Estate, Western Cape, South Africa*, 2004.
- [27] A. Voicila, D. Declercq, F. Verdier, M. Fossorier, and P. Urard, "Low-Complexity Decoding for Non-Binary LDPC Codes in High Order Fields," *IEEE Trans. Commun.*, vol. 58, no. 5, pp. 1365–1375, 2010.
- [28] A. Bennatan and D. Burshtein, "Design and Analysis of Nonbinary LDPC Codes for Arbitrary Discrete-Memoryless Channels," *IEEE Trans. Inf. Theory*, vol. 52, no. 2, pp. 549–583, 2006.
- [29] G. Li, I. J. Fair, and W. A. Krzymien, "Density Evolution for Nonbinary LDPC Codes Under Gaussian Approximation," *IEEE Trans. Inf. Theory*, vol. 55, no. 3, pp. 997–1015, 2009.
- [30] B. M. Kurkoski, K. Yamaguchi, and K. Kobayashi, "Single-Gaussian Messages and Noise Thresholds for Decoding Low-Density Lattice Codes," in *Proc. of IEEE ISIT 2009*, 2009, pp. 734–738.
- [31] H. Uchikawa, B. M. Kurkoski, K. Kasai, and K. Sakaniwa, "Threshold Improvement of Low-Density Lattice Codes via Spatial Coupling," in *Proc. of ICNC 2012*, 2012, pp. 1036–1040.
- [32] M. C. Davey, "Error-Correction using Low-Density Parity-Check Codes," Ph.D. dissertation, University of Cambridge, 2000.